university of groningen / faculty of science and engineering

Investigation of sytematic effects within the BaF eEDM experiment

Bachelor Thesis

Author
Hielke Hoekstra

First Examiner
Prof. dr. K.H.K.J. Jungmann
Second Examiner
Prof. dr. S. Hoekstra
Supervisor
T.B. Meijknecht

June 26, 2020

Abstract

In search for physics beyond the Standard Model the Nl-eEDM collaboration uses a beam of BaF molecules to look for the electric dipole moment of the electron (eEDM). A sensitivity of $5 \cdot 10^{-30}$ e cm is aimed at. In order to reach that sensitivity knowledge and control of numerous systematic effects down to that same sensitivity is essential. The effects of Johnson noise, motional fields and leakage currents have been analyzed and a potential total false eEDM signal due to these effects of $1.4 \cdot 10^{-30}$ e cm has been found.

Contents

1 Introduction **3**

2 Determining the electron EDM **6**
2.1 Theoretical background 6
2.2 Schiff's Theorem 7

3 Investigation of important systematic uncertainties **9**
3.1 Johnson noise 9
3.2 Motional Fields 10
3.3 Leakage currents 11
3.3.1 Macor brackets 12
3.3.2 Coax cables 12
3.3.3 Electric field plates 13
3.3.4 Electric field reversal 14

4 Discussion **14**

5 Acknowledgements **15**

1 Introduction

One of the major achievements in physics in the 20th century is the development of the Standard Model. The Standard Model unified the electromagnetic, weak and strong interactions, only leaving out the fourth fundamental force, gravity [1]. The Standard Model is believed to be self-consistent and succesfully predicted the existence of the W, $Z^{\pm}$ and Higgs bosons, the gluon and the top and charm quarks [2]. However despite its successes there are things the Standard Model can't explain, such as neutrino oscillations, the nature of dark matter and dark energy and the matter-antimatter asymmetry in the universe [3]. One of the necessary conditions to explain the matter-antimatter asymmetry in the universe is the violation of CP-symmetry [4]. Due to CPT-symmetry a violation of CP-symmetry demands violation of T-symmetry. C, P and T denote the corresponding mathematical operations:

- Charge conjugation: invert the sign of all quantum charges ($+ \rightarrow -$)
- Parity transformation: invert the sign of all spacial coordinates ($x \rightarrow -x$)
- Time reversal: invert time ($t \rightarrow -t$)

CPT is generally accepted to be invariant because it follows from the basic assumptions of quantum mechanics, Lorentz invariance and that particle interactions are represented by fields [5]. Within the Standard Model there are CP-violating mechanisms, these, however are insufficient by orders of magnitude to explain the matter-antimatter asymmetry [6]. One such CP violation within the Standard Model is the 2π decay of the K_2^0 meson [7]. Because the Standard Model comes short in explaining the matter-antimatter asymmetry much effort is put in to find additional sources of CP-symmetry or equivalently T-symmetry violation. One type of experiment looking for this asymmetry is the search for permanent electric dipole moments, for example of the electron (eEDM). To understand why a permanent EDM violates

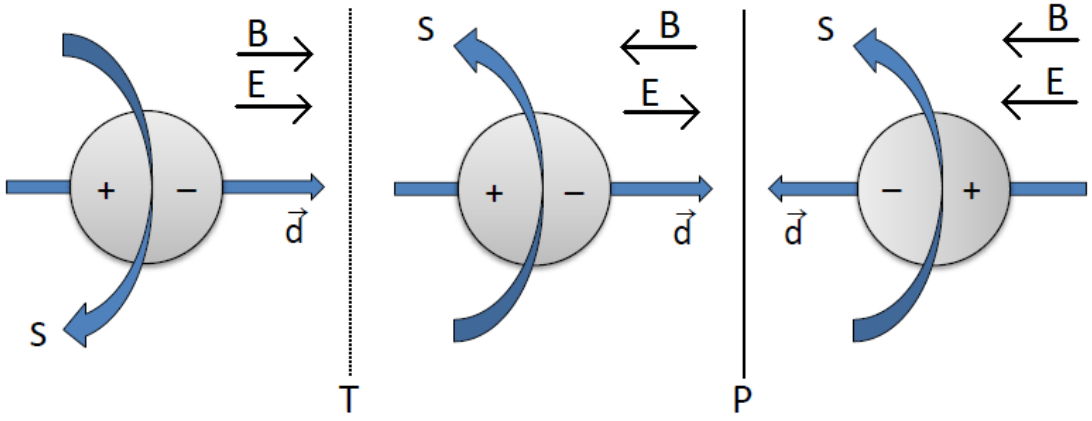

Figure 1: (Left panel) A fundamental particle with spin S and electric dipole d in an electric field E and a magnetic field B. (Middle panel) A fundamental particle with spin S and electric dipole d in an electric field E and a magnetic field B with T applied to it. (Right panel) A fundamental particle with spin S and electric dipole d in an electric field E and a magnetic field B with T and P applied to it. The relative orientation of S and d changes with either T or P applied to the particle. Adapted from [8]

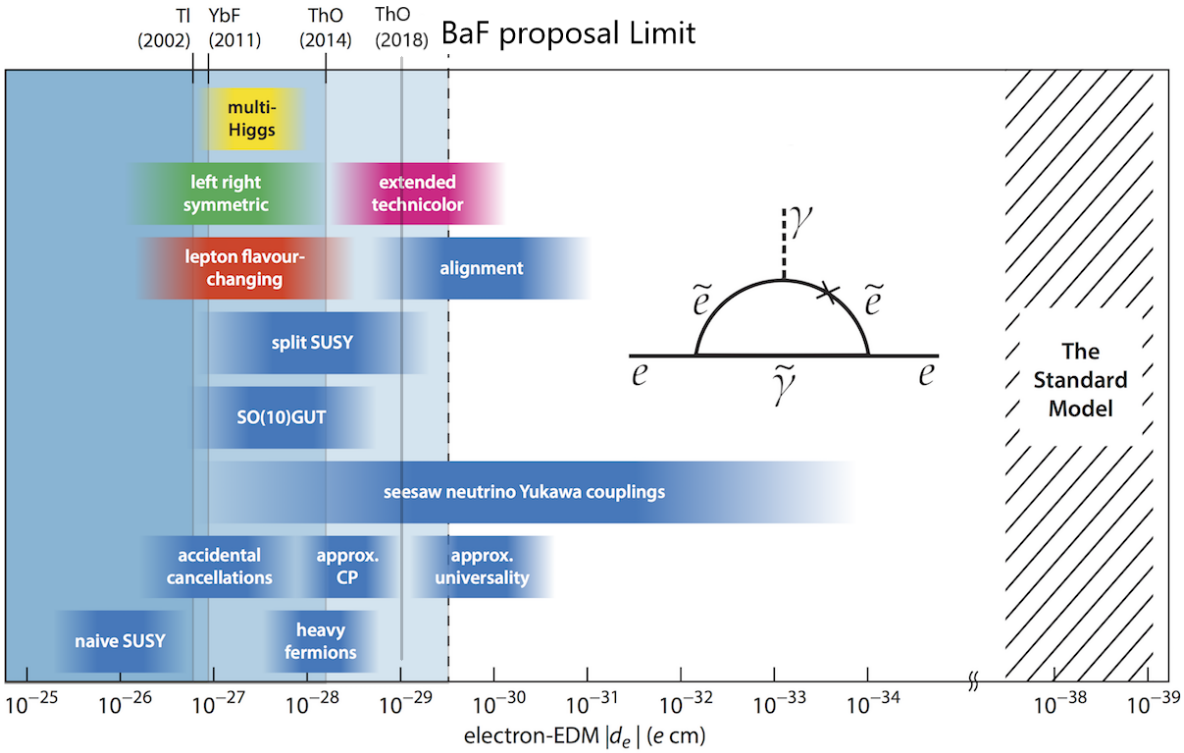

Figure 2: Various theoretical extensions of the Standard Model and the corresponding EDM values are indicated by the colored bars. The experimental upper limits are indicated with the vertical lines and the upper limit of the NL-eEDM is indicated with the dotted line. Figure form [12]

CP consider the situation in figure 1. The EDM d and spin S are parallel aligned, but with the application of either P or T the relative orientation of the EDM and the spin becomes anti-parallel. These particles with parallel and anti-parallel orientations could be distinguished in an electric and magnetic field, however this cannot be for indistinguishable fundamental particles such as electrons and thus, if these particles are found to have an EDM they must violate CP-symmetry [9]. In the Standard Model the eEDM is $d_e = \mathcal{O}(10^{-38})$ which is far out of reach in current experiments, however extensions of the Standard Model, such as supersymmetry (SUSY) predict eEDM values within measurable limits [6], see figure 2 This prospect of new physics to be discovered is the motivation behind the active field of EDM searches. The current upper limit of the eEDM is set by ACME II at $|d_e| < 1.1 \cdot 10^{-29}\,\mathrm{e\,cm}$ [10]. The ongoing experiment of the NL-eEDM collaboration is proposed to be sensitive of eEDM values of $d_e = 5 \cdot 10^{-30}\,\mathrm{e\,cm}$ as can be seen in figure 2 [6]. In order to reach the proposed statistical sensitivity control and understanding of systematic effects is vital. A non-exhaustive list of systematic effects is given in table 1.

This thesis discusses two systematic errors which are deemed important to understand: motional fields and leakage currents. Also a small correction to the statistical sensitivity due to Johnson noise is made.

Table 1: Table of systematic effects. Category I parameters are parameters which ideally are zero. Category II parameters do not have single ideal value and limits of their systematic effect cannot be derived, but they could act as a check of unanticipated systematic effects. Bullet points signify specific possible causes for the parameter above and the cursive effects signify the effects scrutinized in this work. The table is adapted from [11]

Category I Parameters	Category II Parameters
Magnetic Fields	**Laser Powers**
- Non-reversing B-field	- Power of preperation/readout lasers
- Transverse B-fields	**Experiment Timing**
- B-field gradients	- X/Y polarization switching rate
- E correlated B-field	- number of molecule pulses averaged per experiment
• *Motional B-field*	trace
• Geometric phase	**Analysis**
• *Leakage current*	- Signal size cuts, asymmetry size cuts, contrast cuts
Electric Fields	- Difference between two PMT detectors
- Non-reversing E-field	- Variation with time within molecule pulse
• warped plates	- Variation with time throughout the full data set
• misalignment	- Search for correlations between all channels of phase,
. - E-field ground offset	contrast and fluorescence signal
Laser Detunings	- Correlations with auxiliary measurements of B-fields,
- State preparation/readout lasers	laser powers, vacuum pressure and temperature
Laser Pointings	
- Change in pointings	
of preparation/readout lasers	
- State readout laser X/Y	
dependent pointing	
Laser Powers	
X/Y dependent state	
readout laser power?	
Molecular Beam Clipping	
- Molecule beam clipping	
along y and z	

2 Determining the electron EDM

2.1 Theoretical background

The electric dipole moment of charges e with a separation $\mathbf{r}$ is

$$\mathbf{d_e} = e \cdot \mathbf{r}. \tag{1}$$

Analogous to the magnetic moment μ which experiences Larmor precession in an external transverse magnetic field, the eEDM precesses in an external transverse electric field. Both moments are aligned with the spin vector $\mathbf{S}$. Their precession frequencies can be added linearly:

$$\omega_{tot} = \omega_B + \omega_E = \frac{g\mu_B B + d_e E}{h}, \tag{2}$$

where B is the external magnetic field and E is an external electric field felt by the electron in the molecule.
The measurement principle is that of an interferometer. The electrons will be optically pumped from the $|F = 0, M_F = 0\rangle$ state to a coherent superposition of the $|1, -1\rangle$ and the $|1, 1\rangle$ states:

$$\Psi = \frac{1}{\sqrt{2}}(|1, 1\rangle + |1, -1\rangle). \tag{3}$$

Because the $|1, -1\rangle$ and the $|1, 1\rangle$ states have anti-parallel spin vectors the phase accumulation in the interaction zone will also be opposite. Thus the wave function after this interaction is

$$\Psi_{EB} = \frac{1}{\sqrt{2}}(e^{i\phi}\,|1, 1\rangle + e^{-i\phi}\,|1, -1\rangle), \tag{4}$$

where

$$\phi = -(\mu_B B \mp d_e E)\tau/\hbar, \tag{5}$$

is the accumulated phase and τ is the time spend in the interaction zone. After the phase accumulation the molecules are transitioned back to the $|0, 0\rangle$ state but this population transfer is influenced by the interference between the $M_F = \pm 1$ states which depends on the accumulated phase. Counting the amount of particles in the $|0, 0\rangle$ state gives a measure of ϕ. In equation 5 the relative sign of the terms describing the magnetic and electric precession describes whether the magnetic field and the electric field are aligned parallel or anti-parallel [13, 14]. By doing the experiment in both alignments and subtracting the phases from each other only the phase caused by the eEDM remains. This phase is given by

$$\phi_E = \frac{d_e E \tau}{\hbar}. \tag{6}$$

The value value of d_e for which we are sensitive can be derived from the statistical limit which for molecular beam experiments is

$$\sigma_d = \frac{\hbar}{e}\frac{1}{|P|E\tau\sqrt{\dot{N}T}}, \tag{7}$$

where P is the polarization of the BaF molecule in the electric field, $\dot{N}$ is the rate of detected molecules and T is the measurement time [6]. The challenge is to get systematic effects below

this statistical limit.
Effects that are of great concern are those that give rise to magnetic fields in the interaction zone and especially those that give rise to magnetic fields which are correlated with the electric field reversal. Equation 6 assumes the phase accumulated due to the magnetic field has dropped out perfectly when the phases before and after the electric field reversal are subtracted, however when there is a part of the magnetic field ΔB which does not reverse then a phase shift $\phi_{\Delta B}$ due to this magnetic field is measured. This phase $\phi_{\Delta B}$ should not supersede ϕ_E which puts a limit on these stray magnetic fields ΔB. A schematic of the experiment proposed by the NL-eEDM colaboration is given in figure 3, note however that the effects in this thesis are calculated for a foregoing fast beam experiment without the decelerator. The magnetic field used in this experiment has a value $B = 600\,\mathrm{pT}$ because this causes a phase shift of $\pi/4$ where the experiment is most sensitive [6].

2.2 Schiff's Theorem

From the previous section it has already become clear that measuring the eEDM requires an electric field. Because free electrons are accelerated in an electric field, using free electrons adds unnecessary complication to an eEDM search. The next natural candidate to use would be an atom. Schiff's theorem [15] showed that the EDM's of the constituent parts of the atom could not be observed by looking at the atom as a whole, taking as a model for the atom a system of electrostatically bound point particles. Schiff however realised in an atom relativistic effects play an important role and nuclei have a finite size. He showed that taking these effects into account the EDM's of the atom's constituent parts can have an observable effect on the atom itself.
Later Sandars [16] discovered that not only taking these effects into account can cause the EDM's to be observable, but these EDM's can even be enhanced in high-Z molecules or in polar molecules. This enhancement is particularly large in molecules with a large polarisation along the internuclear axis, which is the case for diatomic molecules with a very electronegative atom such as fluorine and a high-Z atom such as Barium. Molecules which are free to rotate in space will have a polarisation averaged to zero. That is why an external electric field is used to align the molecule. It is common to write this enhancement as an effective electric field E_{eff}. Calculating E_{eff} is a highly non-trivial task, however it has been done for many molecules of interest [17]. The lower bound of E_{eff} for BaF is $6\,\mathrm{GV/cm}$ aligned in an external electric field $E_z = 10\,\mathrm{kV}$ [6].

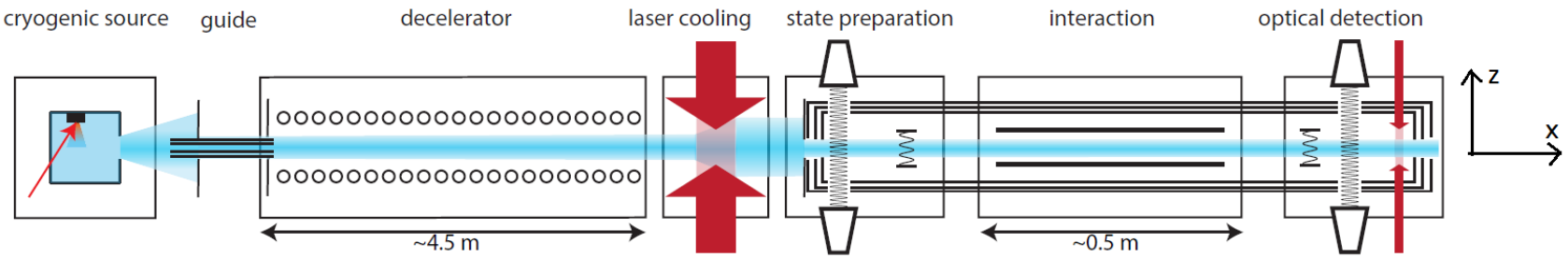

Figure 3: BaF molecules are produced in a cryogenic source. They are decelerated from a 180 m/s to 30 m/s in a decelerator. In the laser cooling zone the transverse velocity of the particles is ±30 m/s preventing the molecules from spreading out in the magnetically shielded interaction zone. The searched for eEDM effect is readout by fluorescence detection in the optical detection region. Figure from [6]

3 Investigation of important systematic uncertainties

We investigate among the potential uncertainties as a first step these, which are considered to have most potential to distort an eEDM experiment on BaF. They are associated with field perturbations seen by a molecular beam. They are known as Johnson noise from the field producing plates and magnetic shielding, motional fields and leakage currents.

3.1 Johnson noise

The following equations and a more elaborate derivation can be found in the work of Devlin et al [21] and its references. A small statistical correction arises from Johnson noise of the electric field plates in the interaction zone and the μ-metal magnetic shielding around this interaction zone. The electric field plates used in the NL-eEDM experiment are 75 cm$\times$10 cm and 1 cm thick soda lime glass plates with a 100 nm conductive IndiumTinOxide (ITO) coating with sheet resistance 300 Ω/sq. The plates are 4cm apart with a voltage of 40kV applied between both plates. The magnetic shielding is a 1.3 m μ-metal cylinder with radius $r = 0.5$ m [19].
Johnson noise is caused by thermal fluctuations of stationary charge carriers in the materials in and around the interaction zone. The statistical uncertainty in the phase introduced by this noise is

$$\sigma_\phi = \frac{\mu_B \tau}{\hbar} \left(\int_0^\infty B_z^2 \frac{\sin^2(\pi f \tau)}{(\pi f \tau)^2} df \right)^{1/2}, \tag{8}$$

where f is the frequency of the noise and B_z for a plate geometry is given by

$$B_z(f) = 2\mu_0 \sqrt{\frac{k_B T}{\pi \rho}} \left(\int_0^\infty R(\xi, d) e^{-2\xi z} \xi d\xi \right)^{1/2}. \tag{9}$$

μ_0 is the vacuum permeability, ρ is the restitivity of the material, $T = 300K$ is the temperature of the material, z is the z-coordinate with the origin at the surface of the electric field plate and $R(\xi, d)$ is taken form [22] in which ξ is a dimensionless variable and d is the thickness of the plates. Johnson noise is white noise (frequency independent) up to frequencies of 10 GHz [23] for our field plates and falls off for higher frequencies, therefore an upper limit of the statistical uncertainty due to Johnson noise is a constant:

$$B_z(0) = \mu_0 \sqrt{\frac{k_B T}{4\pi \rho} \frac{d}{z(z+d)}}. \tag{10}$$

Table 2: The Johnson noise limit σ_d due to the materials of the electric field plates. $\rho = 1 \cdot 10^4\,\Omega\,\mathrm{m}$ [18], $\rho = 3 \cdot 10^{-5}\,\Omega\,\mathrm{m}$ [19] and $\rho = 6 \cdot 10^{-7}\,\Omega\,\mathrm{m}$[20] were used for the soda lime glass, the ITO layer and μ-metal respectively.

	soda lime glass	ITO	μ-metal
E-field plates	$2.3 \cdot 10^{-34}\,\mathrm{e\,cm}$	$1.6 \cdot 10^{-32}\,\mathrm{e\,cm}$	
Magnetic shielding			$7.6 \cdot 10^{-31}\,\mathrm{e\,cm}$

This yields the phase noise per measurement. This converts to the statistical uncertainty for the experiment as

$$\sigma_d = \frac{\sigma_\phi \hbar}{\tau E_{eff}\sqrt{N}}, \tag{11}$$

where $N = 9 \cdot 10^5$ [6] is the number of molecules in the entire experiment. Romalis and Lee [24] have devised in similar fashion an expression for the magnetic field caused by Johnson noise from cylindrical high permeability magnetic shields. The Johnson noise uncertainty is listed in table 2 and is safe to neglect in the present experimental limit.

3.2 Motional Fields

If a particle moves through a electromagnetic field with velocity v it will not only feel the laboratory electromagnetic field but also an additional motional electromagnetic field associated with the Lorentz transform of the laboratory field into the particle's frame

$$\mathbf{E_{mot}} = \mathbf{v} \times \mathbf{B}, \tag{12}$$

$$\mathbf{B_{mot}} = \frac{\mathbf{v} \times \mathbf{E}}{c^2}. \tag{13}$$

Note, E is the laboratory electric field not the effective electric field E_{eff}. The magnetic field used in the experiment is 600 pT which gives $E_{mot} = 4 \cdot 10^{-26}\,\mathrm{V/cm}$, which is safe to neglect, however the motional magnetic field is of the order of 5 nT and thus requires further investigation.
It is known through perturbation theory that the effects of perpendicular magnetic fields such as motional magnetic fields are strongly suppressed by the large Stark splitting between the $|1, \pm 1\rangle$ and $|1, 0\rangle$ levels [25]. This Stark splitting for the BaF molecule is given by [26]

$$\Delta = 14.01\,\mathrm{kHz/(kV/cm)^2} E^2. \tag{14}$$

This perturbation theory ansatz in [25] assumes the perpendicular field B_p is significantly smaller than the produced magnetic field B_z, which in this experiment is not true for the motional magnetic field. Therefore the effect of perpendicular magnetic fields is analysed by means of diagonalizing the associated Hamiltonian matrix [14]

$$H = \Delta + \mu_B(B_z\sigma_z + B_p\sigma_x) = \begin{pmatrix} \Delta + \mu_b B_z & \mu_b \frac{B_p}{\sqrt{2}} & 0 \\ \mu_b \frac{B_p}{\sqrt{2}} & 0 & \mu_b \frac{B_p}{\sqrt{2}} \\ 0 & \mu_b \frac{B_p}{\sqrt{2}} & \Delta - \mu_b B_z \end{pmatrix}. \tag{15}$$

The three energy eigenvalues of equation 15 can be found in appendix A. These energy eigenvalues were evaluated in Python for both electric field orientations. Then $\mathcal{E}_+ - \mathcal{E}_-$ in the parallel orientation and $\mathcal{E}_+ - \mathcal{E}_-$ in the anti-parallel orientation were subtracted from each other, because this is what is measured. As one might expect in the perfect experiment in which the E is perfectly reversed, each shot has the same velocity and everything is perfectly aligned the effect of the motional field is exactly zero because it drops out just like ϕ_{B_z}.
A systematic error arises when there is an asymmetry in the motional field before and after the electric field reversal. This asymmetry can arise due to an incomplete reversal of the electric

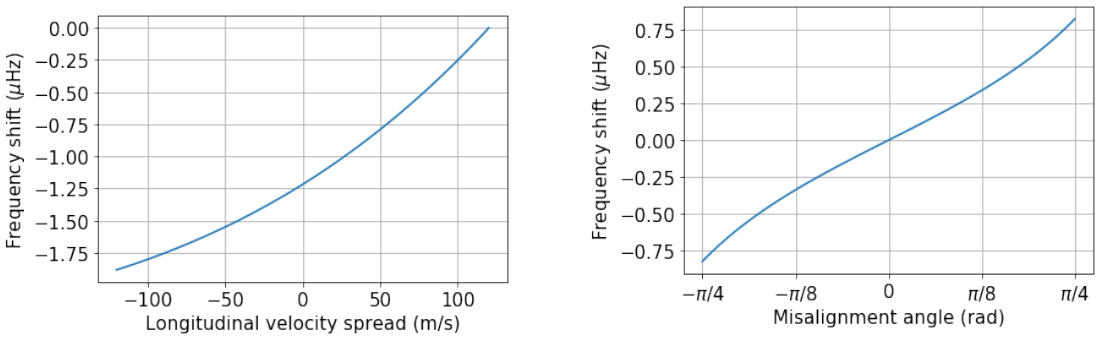

Figure 4: Motional fields cause frequency shifts. Here the effects are displayed for $v = 600\,\mathrm{m/s}$, $B = 600\,\mathrm{pT}$ and $E = 10\,\mathrm{kV}$.(a) The measured frequency shift due to B_{mot} as a function of the velocity spread. The plot is generated with a velocity increased by 20% when the magnetic and electric field are aligned parallel, the velocity spread is ±20% in the anti-parallel alignment. (b) The measured frequency shift due to B_{mot} in conjunction with a misalignment of the electric and magnetic field as function of the misalignment angle between the electric and magnetic field

field or difference in the velocity of the molecules before and after the electric field reversal. The non-reversing part of the electric field is expected to be small, but the velocity spread is around 20% of the average value [6]. This velocity spread in the anti-parallel alignment of the electric and magnetic field is plotted in figure 4a in the absolute worst case scenario where all molecules measured in the parallel alignment of the electric and magnetic field have a velocity 20% higher than the expected average velocity. In the figures it can be seen that in the unlikely scenario where the particles in the parallel situation have a 20% increased velocity and in the anti-parallel situation have 20% decreased velocity the maximum frequency is less than 2 µHz which is well below the 7 µHz statistical noise.

Another way in which the motional field could produce a systematic effect is in association with a misalignment between the electric and magnetic field. When the magnetic field is not perfectly aligned with the electric field it will have a component in the direction parallel to the motional field. This causes an asymmetry in the perpendicular magnetic field felt by the molecules upon switching the electric field. In figure 4b the frequency shift due to this misalignment is plotted as a function of the misalignment angle. Even for an extreme misalignment of $\pi/4$ the frequency shift is at most a fraction of a µHz which is again well below the statistical limit.

3.3 Leakage currents

It is readily known through Ampère's law that a current causes a magnetic field. Because the nl-eEDM experiment is sensitive to magnetic field parallel to the electric field down to the fT scale this puts very stringent restrictions on the currents that can flow close to the interaction zone.

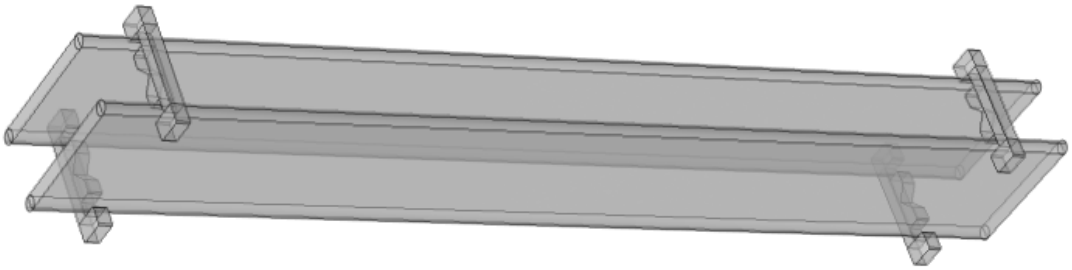

Figure 5: COMSOL model of the electric field plates and its brackets. The electric field plates have dimensions 75 cm×10 cm×1 cm and are upheld in the vacuum system by four brackets made from Macor.

In figure 5 COMSOL drawings of the electric field plate set-up are shown. The brackets are made of a glass ceramic, Macor[19], which according to the manufacturer has a volume resistivity of $\rho = 1 \cdot 10^{17}\,\Omega\,\mathrm{cm}$ at room temperature[27]. This COMSOL model was used to evaluate how much current is flowing through this bracket by performing a surface current integral on a plane in between the electric field plates. It is $I = 7.2 \cdot 10^{-17}\,\mathrm{A}$. To get an order of magnitude of the magnetic field produced by this current the Biot-Savart law for a solid cylinder is used

$$B = \frac{\mu_0 I}{2\pi r}, \tag{16}$$

where r is the distance to the bracket, $r > 4\,\mathrm{cm}$. This yields $B = 3.6 \cdot 10^{-22}\,\mathrm{T}$ which corresponds to a Larmor precession of $2.6 \cdot 10^{-14}\,\mathrm{rad}$. During installation great care should be put in to not get moisture, grease or other contamination on the brackets because that could provide for a low resistance path over the brackets rather than through the brackets.

3.3.2 Coax cables

Another possible source of leakage currents is through the dielectric of the coax cables used to charge the electric field plates. In order to calculate this leakage current the resistance of the cable is determined with the following equation (see appendix B)

$$R = \frac{\rho}{2\pi L} \ln\left(\frac{b}{a}\right), \tag{17}$$

where ρ is the resistivity of the dielectric, $L = 5\,\mathrm{m}$, b is the radius of the outer conductor and a is the radius of the inner conductor. $\ln(b/a)$ is typically somewhere between 1 and 2 and many coax cables have PE or PTFE as dielectrics which have resistivities of about $10^{17}\,\Omega\,\mathrm{cm}$. Combined with Ohm's law and a voltage of 30000V the radial current is $6.3 \cdot 10^{-13}\,\mathrm{A}$. The Larmor precession resulting from this current is $4.6 \cdot 10^{-10}\,\mathrm{rad}$.

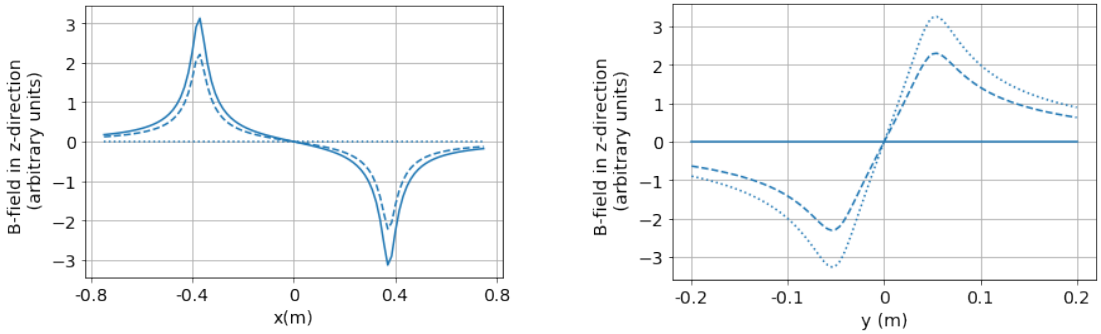

(a) **(b)**

Figure 6: Numerical integration of equation 18 without constants with the origin of the axis-system in the middle between the plates. (solid) $\hat{K} = \hat{y}$, (dashes) $\hat{K} = 1/\sqrt{2}\,\hat{x} + 1/\sqrt{2}\,\hat{y}$, (dots) $\hat{K} = \hat{x}$. (a) The magnitude of the magnetic field in the z-direction along the x-direction. (b) The magnitude of the magnetic field in the z-direction along the y-direction.

3.3.3 Electric field plates

Currents can also flow on the electric field plates themselves. The magnetic field which results from this current with surface current density $\mathbf{K}(\mathbf{r}')$ at a point $\mathbf{r}$ is given by Biot-Savart law

$$B = \frac{\mu_0 K}{4\pi} \int\int dx'dy' \frac{\hat{\mathbf{K}} \times (\mathbf{r} - \mathbf{r}')}{|\mathbf{r} - \mathbf{r}'|^3}. \tag{18}$$

Different numerical integrations of equation 18 are shown in figure 6. The x-direction is defined in the length of the plates and the y-direction is defined in the height of the plates. Figure 6 gives the magnetic field in the z-direction. The magnetic field perpendicular to the magnetic field in the z-direction is of the same order of magnitude but the Larmor precession due to such a perpendicular magnetic field is heavily suppressed by the Stark shift as stated in section 4.2 and is therefore neglected. From figure 6b we can conclude that in order to keep the effect of a current on the plates as low as possible the molecular beam should be aligned in the middle of the plates. In order to keep the effects of a non-reversing magnetic field below the statistical limit any unwanted magnetic field in the z-direction should have a magnitude of less than 0.5 fT. From equation 18 a maximum 'allowed' current of order 10^{-9} A is derived.
One possible cause for currents to flow on the electric field plates is by the Seebeck thermoelectric effect [28]. A voltage V is induced in proportion to the temperature gradient ΔT.

$$V = S\Delta T, \tag{19}$$

where S is the Seebeck coefficient. The Seebeck coefficient of the ITO layer is around $30\,\mu\mathrm{V\,K^{-1}}$ at room temperature [29]. From Ohm's law, a sheet resistance of $300\,\Omega/\mathrm{sq}$ and the aforementioned maximum current the temperature difference between both ends of the plates cannot not exceed 0.4 K. Since the experiment is executed in an enclosed vacuum system this seems achievable.

3.3.4 Electric field reversal

Another current arises when the electric field is reversed. During the discharging and recharging of the electric field plates a current flows through the coax cables which produce a magnetic field. This current is given by (see appendix C)

$$I = \frac{V}{R} e^{\frac{-t}{\tau}}, \tag{20}$$

where t is time, V is the initial voltage on the plates, R is the resistance of the circuit and $\tau = RC$ is the time constant with C the capacitance. R is the resistance of the total circuit but the resistance of the cables and the ITO coating are small compared to the 3 MΩ internal resistance of the iseg 300W HPS and are therefore neglected. The capacitance of the electric field plates is

$$C = \frac{\epsilon_0 A}{d}, \tag{21}$$

where ϵ_0 is the vacuum permittivity, A is the area of the plates and d is the distance between the plates. Within 2 ms, $I < 4 \cdot 10^{-20}$ A in the cables, which is below the thermal noise limit.

4 Discussion

Table 3: All false eEDM values of systematic effects discussed in this thesis, upper limits of the current and temperature gradient on the electric field plates and minimum time between restarting measurements after electric field reversal.

Johnson noise	$7.6 \cdot 10^{-31}$ e cm
Motional fields	$1.2 \cdot 10^{-30}$ e cm
Macor brackets	$3.4 \cdot 10^{-34}$ e cm
Coax cables	$6.1 \cdot 10^{-32}$ e cm
Total	$1.4 \cdot 10^{-30}$ e cm
Current on E-field plates	$I < 10^{-9}$ A and $\Delta T < 0.4$ K
E-field reversal	$t > 10$ µs

In table 3 a list of all the false eEDM values of the systematic effects and requirements on parameters discussed in this thesis are given. Because all systematic effects discussed in this work are assumed to be independent, therefore all systematic effects can be added in quadrature which yields a total false eEDM value of $1.4 \cdot 10^{-30}$ e cm which is 28% of the statistical sensitivity. Since there are still a lot of systematic effects in table 1 which will add to the total tally of systematic errors it might turn out essential to reduce the systematic effects investigated in this thesis even further. The main contributors to the false eEDM found in this thesis are the Johnson noise of the magnetic shielding and the motional magnetic field. The mu-metal magnetic shielding is the biggest integral part of the set-up and thus replacement of this shielding will only be a viable upgrade in the far future. However the largest systematic effect –the motional fields– has been calculated for a fast beam experiment with the molecules travelling $v = 600$ m/s. The future prospect of the BaF eEDM experiment however is to do the experiment with a molecular beam with $v = 30$ m/s which will reduce the false eEDM due to the motional field 20-fold.

Although the effects of leakage currents in the macor brackets and the coax cables is negligible in ideal circumstances, to work as careful and cleanly with them as possible because any damage done to these components or any contamination on these components could increase the false eEDM signal by orders of magnitude.

All values derived in this thesis are based on theory and calculation alone because during the duration of this thesis access to the lab was strictly prohibited and thus no measurements could be carried out. To add to the confidence about the knowledge and control of these particular systematic effects and also other systematic effects in table 1 many measurements have to be carried out. For example measurements of the longitudinal velocity distribution are essential to account for motional field effects and leakage currents can directly be measured. Also correct alignment of various components in the set-up is essential for the experiment to work correctly.

Accurate knowledge of the systematic effects at play and careful measurements of these systematic effects could in the end also help not only to account for systematic effects but even correct for systematic effects similar to Kara et al [30].

5 Acknowledgements

I would like to thank the complete FIS group and VSI for making me feel like a part of the team for the duration of my bachelor's thesis even in these weird times dominated by the covid 19 virus. Also many thanks to the fast beam group for their weekly interests in my project that kept me motivated to progress during these 10 weeks.
I especially thank Klaus Jungmann, Lorenz Willmann, Thomas Meijknecht and fellow bachelor student Maarten Mijland for their countless meetings and discussions. Without their support and guidance this project would not have been what it is today.
My final thanks go to my parents for taking me back in and providing for me during these weird times.

References

[1] T. Shears, "The standard model", Philosophical Transactions of the Royal Society A **370**, 805–817 (2012).

[2] J. Woithe, G. Wiener, and F. Van der Veken, "Let's have a coffee with the standard model of particle physics!", Physics Education **52**, 1–9 (2012).

[3] R. Oerter, *The theory of almost everything: the standard model, the unsung triumph of modern physics* (Pi Press, 2005).

[4] A. Sakharov, "Violation of cp invariance, c asymmetry, and baryon asymmetry of the universe", Journal of Experimental and Theoretical Physics Letters **5**, 24–27 (1967).

[5] G. Lüders, "Proof of the tcp theorem", Annals of Physics **2**, 1–15 (1957).

[6] P. Aggarwal, H. Bethlem, A. Borschevsky, M. Denis, K. Esajas, P. Hase, Y. Hao, S. Hoekstra, K. Jungmann, T. Meijknecht, M. Mooij, R. Timmermans, W. Ubachs, L. Willmann, and A. Zapara, "Measuring the electric dipole moment of the electron in baf", The European Physical Journal D **72** (2018).

[7] J. Christenson, J. Cronin, V. Fitch, and R. Turlay, "Evidence for the 2π decay of the k_2^0 meson", Physical Review Letters **13**, 138–140 (1964).

[8] N. Hutzler, "A new limit on the electron electric dipole moment: beam production, data interpretation, and systematics", PhD thesis (Harvard University, Feb. 2014).

[9] B. Roberts and W. J. Marciano, *Lepton dipole moments* (World Scientific, 2010).

[10] V. Andreev, D. Ang, J. Doyle, G. Gabrielse, J. Haefner, N. Hutzler, C. Meisenhelder, C. Panda, E. West, X. Wu, D. DeMille, Z. Lasner, B. O'Leary, and A. West, "Improved limit on the electric dipole moment of the electron", Nature **562**, 355–360 (2018).

[11] B. R. O'Leary, "In search of the electron's electric dipole moment in thorium monoxide: an improved upper limit, systematic error models, and apparatus upgrades", PhD thesis (Yale University, Dec. 2016).

[12] R. Borchers, "Investigation on different sources of magnetic noise on the sensitivity of the baf eedm experiment.", Bachelor's thesis (Rijksuniversiteit Groningen, 2019).

[13] P. Condylis, "Measuring the electron electric dipole moment using supersonic ybf", PhD thesis (Imperial College London, Feb. 2006).

[14] J. Hudson, "Measuring the electric dipole moment of the electron with ybf molecules", PhD thesis (University of Sussex, Sept. 2001).

[15] L. Schiff, "Measurability of nuclear electric dipole moments", Physical Review **132**, 2194 (1963).

[16] P. Sandars, "The electric dipole moment of an atom", Physical Review Letters **14**, 194 (1965).

[17] M. Abe, V. Prasannaa, and B. Das, "Application of the finite-field coupled-cluster method to calculate molecular properties relevant to electron electric-dipole-moment searches", Physical Review A **97**, 032515 (2018).

[18] C. J. Munger, "Magnetic johnson noise constraints on electron electric dipole moment experiments", Physical Review A **72** (2004).

[19] O. Boll, private communication.

[20] *Mumetal properties*, `http://www.mu-metal.com/technical-data.html` (visited on 06/21/2020).

[21] I. Rabey, J. Devlin, E. Hinds, and B. Sauer, "Low magnetic johnson noise electric field plates for precision measurement", review of scientific instruments **87** (2016).

[22]T. Varpula and T. Poutanen, "Magnetic field fluctuations arising from thermal motion of electric charge in conductors", Journal of Applied Physics **55** (1984).
[23]J. Nenonen, J. Montonen, and T. Katila, "Thermal noise in biomagnetic measurements", Review of Scientific Instruments **67**, 2399 (1994).
[24]S.-K. Lee and M. Romalis, "Calculation of magnetic field noise from high-permeability magnetic shields and conducting objects with simple geometry", Journal of Applied Physics **103**, 084904.1–10 (2008).
[25]M. Sandars and P. Player, "An experiment to search for an electric dipole moment in the $^3p_2$ metastable state of xenon", Journal of Physics B **3**, 1621–1623 (1970).
[26]A. Vutha, M. Horbatsch, and E. Hessels, "Orientation-dependent hyperfine structure of polar molecules in a rare-gas matrix: a scheme for measuring the electron electric dipole moment", Physical Review A **98** (2018).
[27]*Macor machinable glass*, `https://www.corning.com/worldwide/en/products/advanced-optics/product-materials/specialty-glass-and-glass-ceramics/glass-ceramics/macor.html` (visited on 06/11/2020).
[28]T. Seebeck, "Magnetische polarisation der metalle und erze durch temperatur-differenz", Abhandlungen der Königlichen Akademie der Wissenschaften zu Berlin, 265–373 (1822).
[29]A. El Amrani, F. Hijazi, B. Lucas, J. Bouclé, and M. Aldissi, "Electronic transport and optical properties of thin oxide films", Thin Solid Films **518**, 4582–4585 (2009).
[30]D. Kara, I. Smallman, J. Hudson, B. Sauer, M. Tarbutt, and E. Hinds, "Measurement ofthe electron's electric dipole moment using ybf molecules: methods and data analysis", New Journal of physics **14** (2012).
[31]Q. Shi and O. Kanoun, "Automated wire fault location using impedance spectroscopy and differential evolution", in (Instrumentation and Measurement Technology Conference (IEEE I2MTC), May 2013), pp. 359–364.

Appendix A: Eigenvalues of a 3×3 Hamiltonian

$$H = \Delta + \mu_B(B_z\sigma_z + B_p\sigma_x) = \begin{pmatrix} \Delta + \mu_b B_z & \mu_b\frac{B_p}{\sqrt{2}} & 0 \\ \mu_b\frac{B_p}{\sqrt{2}} & 0 & \mu_b\frac{B_p}{\sqrt{2}} \\ 0 & \mu_b\frac{B_p}{\sqrt{2}} & \Delta - \mu_b B_z \end{pmatrix} \tag{A.1}$$

Finding the eigenvalues of the Hamiltonian given by equation A.1 amounts to finding the third degree polynomial

$$x^3 - 2\Delta x^2 + (\Delta^2 - B_z^2 - B_p^2)x + \Delta B_p^2 = 0. \tag{A.2}$$

Now take $a = -2\Delta$, $b = \Delta^2 - B_z^2 - B_p^2$ and $c = \Delta B_p^2$, so

$$x^3 + ax^2 + bx + c = 0. \tag{A.3}$$

Let $x = A\cos(\theta) + B$ and use the triple angle formula to find

$$\frac{1}{4}A(8aB + 3A^2 + 4b + 12B^2)\sin(\theta) + A^2(a+3B)\sin^2(\theta) - \frac{1}{4}A^3\sin(3\theta) + aB^2 + bB + B^3 + c = 0. \tag{A.4}$$

Now choose A and B such that $8aB + 3A^2 + 4b + 12B^2 = 0$ and $a + 3B = 0$ and the equation becomes

$$\frac{1}{27}(2a^3 - 9ab + 27c) - \frac{2}{27}(a^3 - 3b)^{3/2}\sin(3\theta) = 0, \tag{A.5}$$

and solving for θ yields

$$\theta = \frac{1}{3}\left(\arcsin\left(\frac{2a^3 - 9ab + 27c}{2(a^2 - 3b)^{3/2}}\right) + 2\pi k\right), \tag{A.6}$$

with $k = -1, 0, 1$. If we now substitute back $a = -2\Delta$, $b = \Delta^2 - B_z^2 - B_p^2$ and $c = \Delta B_p^2$ and solve for x we find

$$x_k = \frac{2}{3}\sqrt{\Delta^2 + 3(B_z^2 + B_p^2)} \sin\left(\frac{1}{3}\arcsin\left(\frac{-16\Delta^3 + 18\Delta(\Delta^2 - B_z^2 - B_p^2) + 27\Delta B_p^2}{2(\Delta^2 + 3(B_z^2 + B_p^2))^{3/2}}\right) - \frac{2\pi}{3}k\right) + \frac{2\Delta}{3}, \tag{A.7}$$

where $k = -1, 0, 1$ correspond to $\mathcal{E}_0$, $\mathcal{E}_-$, $\mathcal{E}_+$ respectively.

Appendix B: Radial resistance of a coax cable

Divide the cable up in infinitesimal concentric shells of thickness dr with resistivity ρ, length L and radius r. The resistance of such an shell is given by

$$dR = \frac{\rho dr}{A} = \frac{\rho dr}{2\pi r L}. \tag{B.1}$$

Integrating from a to b yields

$$R = \int_a^b \frac{\rho dr}{2\pi r L} = \frac{\rho}{2\pi L} \ln\left(\frac{b}{a}\right) \tag{B.2}$$

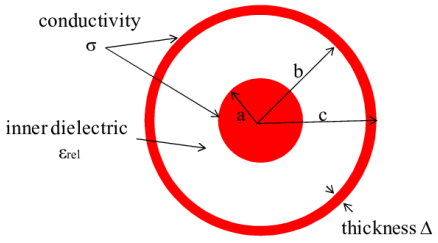

Figure B.1: A coaxial cable with an inner conductor with radius a and conductivity σ and an outer conductor with radius b, thickness Δ and conductivity σ with an dielectric layer with a relative permittivity ϵ_{rel}. From [31]

Appendix C: Charging capacitor

In figure C.1 the voltage V_0 is given by the sum of the voltages across the resistor with resistance R and the capacitor with capacitance C. The voltage on the capacitance results from charge accumulation on the electrodes of the capacitor, thus the voltage on capacitor is the time integral over the current. V_0 is given by

$$V_0 = V_R + V_C = I(t)R + \frac{1}{C}\int_{t_0}^{t} I(\tau)d\tau. \tag{C.1}$$

Taking the derivative and multiplying with C yields a first order differential equation,

$$RC\frac{\mathrm{d}I(t)}{\mathrm{d}t} + I(t) = 0, \tag{C.2}$$

which is easily solved with the initial conditions at $t = 0$ there is no voltage across the capacitor and the initial current is $I(0) = V_0/R$. The result we obtain is

$$I(t) = \frac{V_0}{C}\, e^{\frac{-t}{\tau}}, \tag{C.3}$$

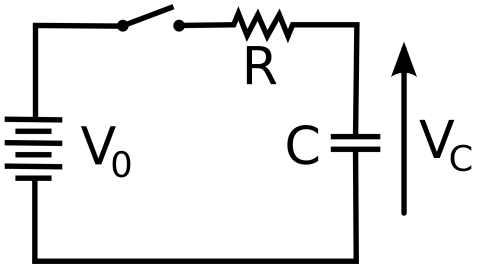

Figure C.1: .

where $\tau = RC$. Equation C.3 gives the current after charging time t. From the derivation above it is straightforward to find the current after discharging time t of a capacitor

$$I(t) = \frac{V_{C_i}}{C}\, e^{\frac{-t}{\tau}}, \tag{C.4}$$

with V_{C_i} the initial charge on the capacitor.